Influence of elastase on alanine-rich peptide hydrogels

ARTICLE *in* BIOMATERIALS SCIENCE · JUNE 2014

Impact Factor: 3.83 · DOI: 10.1039/c4bm00001c

Biomaterials Science

PAPER

View Article Online
View Journal | View Issue

Cite this: *Biomater. Sci.*, 2014, **2**, 867

Influence of elastase on alanine-rich peptide hydrogels

V. Castelletto,[a] R. J. Gouveia,[a] C. J. Connon,[a] I. W. Hamley,*[a] J. Seitsonen,[b] J. Ruokolainen,[b] E. Longo[c] and G. Siligardi[c]

Received 2nd January 2014,
Accepted 23rd January 2014

DOI: 10.1039/c4bm00001c

www.rsc.org/biomaterialsscience

The self-assembly of the alanine-rich amphiphilic peptides Lys(Ala)$_6$Lys (KA_6K) and Lys(Ala)$_6$Glu (KA_6E) with homotelechelic or heterotelechelic charged termini respectively has been investigated in aqueous solution. These peptides contain hexa-alanine sequences designed to serve as substrates for the enzyme elastase. Electrostatic repulsion of the lysine termini in KA_6K prevents self-assembly, whereas in contrast KA_6E is observed, through electron microscopy, to form tape-like fibrils, which based on X-ray scattering contain layers of thickness equal to the molecular length. The alanine residues enable efficient packing of the side-chains in a beta-sheet structure, as revealed by circular dichroism, FTIR and X-ray diffraction experiments. In buffer, KA_6E is able to form hydrogels at sufficiently high concentration. These were used as substrates for elastase, and enzyme-induced de-gelation was observed due to the disruption of the beta-sheet fibrillar network. We propose that hydrogels of the simple designed amphiphilic peptide KA_6E may serve as model substrates for elastase and this could ultimately lead to applications in biomedicine and regenerative medicine.

Introduction

A major challenge in regenerative medicine is to create mimics of the extracellular matrix (ECM). To enable dynamic remodelling of ECM-mimics, substrates for proteases can be included. One example is the incorporation of substrates for elastase, which are often alanine-rich short peptides.[1] Elastase plays an important role in tissue injury[2] and elastase inhibitors are of interest for applications in wound healing, among others,[3] since elastase degrades elastin within the natural connective tissue. Elastin, as its name suggests, provides elasticity, for example to the skin. Alanine-rich sequences are found within certain exons of elastin[4] The conformations of synthetic alanine-rich peptides such as Ac-$A_4KA_4KA_4KA$-NH_2[5] and Ac-KKA_7KK-NH_2[6] and Ac-KKA_7EE-NH_2[6] have been examined by circular dichroism (CD) spectroscopy and NMR techniques. Elastase-sensitive substrates such as A_9K have been incorporated into PEG hydrogels to enable the creation of proteolytically-degradable materials for cell culturing.[1a,7] Another important biological role of alanine-rich sequences is found in spider silk where alanine repeats containing 5–7 residues are observed in major ampullate Spidroin 1, separated by repeats of a GGX motif.[8] The alanine-rich domain forms tightly packed β-sheet structures which contribute to the exceptional tensile strength of spider silk.[8b]

Surfactant-like peptides based on linked sequences of hydrophobic residues attached to shorter charged residue "headgroups" were introduced by Zhang and co-workers.[9] Stupp and co-workers examined the self-assembly of a lipopeptide C_{16}-A_6E_3 incorporating an A_6 sequence, and observed X-ray induced ordering of filaments into ordered bundles.[10] We recently examined the self-assembly of the mono-capped alanine-rich peptide A_6K into nanotubes,[11] following earlier work on the self-assembly of this peptide.[12] In an initial model, based on (what we now believe to be incorrect) constraints from prior SAXS studies, we presented a model in which peptide β-strands were aligned parallel to the nanotube walls.[11] Based on data obtained from solid-state NMR experiments along with FTIR on isotope-labelled peptides, we have now shown that the peptides are in fact aligned perpendicular to the nanotube walls.[13] We reasoned that analogous peptides capped at both ends with oppositely charged termini would be likely to form hydrogels due to favorable electrostatic interactions and here we report on the self-assembly of KA_6E which has oppositely charged residues at the termini as well as the "homo-telechelic" peptide KA_6K. These short model peptides undergo distinct self-assembly behaviour, including, in the case of KA_6E, hydrogelation. In addition, we examine the response of the hydrogel to degradation by elastase.

[a]*School of Chemistry, Food Biosciences and Pharmacy, University of Reading, Whiteknights, Reading RG6 6AD, UK. E-mail: I.W.Hamley@reading.ac.uk*
[b]*Department of Applied Physics, Aalto University School of Science, P.O. Box 15100, FI-00076 Aalto, Finland*
[c]*Diamond Light Source Ltd, Harwell Science and Innovation campus, Didcot, Oxfordshire OX11 0DE, UK*

Oligo-alanine peptides containing fewer than nine alanine residues are observed to form β-sheet structures, whereas longer sequences (in the range 9–19 studied) leads to the formation of a mixed α-helical/β-sheet structure.[14] Therefore, KA_6E is expected to adopt a β-sheet conformation. On the other hand, other groups report that alanine-rich peptides with charged terminal residues can adopt folded conformations such as polyproline II.[15] The secondary structure of the KA_6E peptide will be analyzed here, along with elastase-induced degradation of hydrogels.

Experimental

Materials

Peptides NH_2-KA_6E-COOH (K: lysine, A: alanine, E: glutamic acid) and NH_2-KA_6K-COOH were custom-synthesized by CS Bio (Menlo Park, USA) as TFA salts. Both termini are uncapped. The peptides will henceforth be termed KA_6E and KA_6K. The purity of the peptides was determined by analytical HPLC in a TFA water/acetonitrile gradient, while the molecular weight M_W was obtained by electrospray-mass spectrometry. KA_6E purity was 98.36%, the molecular weight was $M_{W,found}$ = 701.67 Da ($M_{W,expected}$ = 701.78 Da). KA_6K purity was 95.81%, the molecular weight was $M_{W,found}$ = 700.67 Da ($M_{W,expected}$ = 700.84 Da). Elastase from porcine pancreas (M_W = 25.9 kDa) and Trizma@ base were purchased from Sigma Aldrich. KA_6K and KA_6E were dissolved in water. It has been reported that elastase solubility increases at pH 8. Then, a Trizma@ base solution (titrated with 1 M HCl to pH 8) was used to dissolve weighed amounts of KA_6E or elastase, during the study of the elastase effects on KA_6E peptide. The molar ratio of elastase to KA_6E used in this work will be indicated as [KA_6E]/[elastase] = Mr_E.

Circular dichroism (CD)

In the lab, spectra were recorded using a Chirascan spectropolarimeter (Applied Photophysics, UK). The sample was placed in a cover slip cuvette (0.01 mm thick). Spectra are presented with absorbance $A < 2$ at any measured point with a 0.5 nm step, 1 nm bandwidth, and 1 second collection time per step at 20 °C. The post-acquisition smoothing tool from Chirascan software was used to remove random noise elements from the averaged spectra. A residual plot was generated for each curve in order to verify whether or not the spectrum has been distorted during the smoothing process. The CD signal from the water was subtracted from the CD data of the peptide solutions.

CD spectra for KA_6E/elastase mixtures were measured at the synchrotron CD beamline B23 (Diamond Light Source, UK).[16] For these experiments, the sample was loaded into a CaF_2 demountable cuvette cell with a 0.01 mm pathlength. The spectra were measured at 20 °C in the far-UV region (260–180 nm) with a 0.5 nm step and 1 second integration time. The CD spectrum of the solvent/buffer was subtracted from the CD spectra of the peptide solutions.

Fourier transform infra-red (FTIR) spectroscopy

Spectra were recorded using a Thermo-Scientific Nicolet IS5 or a Nexus-FTIR spectrometer, both equipped with a DTGS detector. Samples were sandwiched between two CaF_2 plate windows (spacer 0.012 or 0.025 mm thick). Spectra were scanned 128 or 168 times over the range of 900–4000 cm^{-1}.

Small-angle X-ray scattering (SAXS)

Experiments were performed on beamline BM29 at the ESRF (Grenoble, France). A few microlitres of samples were injected *via* an automated sample exchanger at a slow and very reproducible flux into a quartz capillary (1.8 mm internal diameter), which was then placed in front of the X-ray beam. The quartz capillary was enclosed in a vacuum chamber, in order to avoid parasitic scattering. After the sample was injected in the capillary and reached the X-ray beam, the flow was stopped during the SAXS data acquisition. The sample was thermostated throughout its entire travel from the injector to the quartz capillary. SAXS experiments were performed at 20 °C. The $q = 4\pi \sin\theta/\lambda$ range was set to 0.004–0.4 $Å^{-1}$, with λ = 1.03 Å (12 keV). The images were captured using a PILATUS 1M detector. Data processing (background subtraction, radial averaging) was performed using dedicated beamline software ISPYB.

SAXS theory

In this work we fitted the SAXS data of KA_6E tapes as a product between the form factor of Gaussian bilayers and the modified Caillé structure factor corresponding to lamellar systems. The details of the bilayer model and the modified Caillé structure factor are given elsewhere.[17] The model for Gaussian bilayers assumes an electron density profile comprising one Gaussian function for each headgroup on either side of the bilayer electron density, (ρ_H), and one Gaussian function for the electron density of the chains in the core of the bilayer (ρ_C). The density ρ_H has peaks centred at z_H and $-z_H$ with width σ_H. The density ρ_C has a peak centred at z_C, with width σ_C. Our model assumes that the bilayer is centred at $z = z_C = 0$. Gaussian polydispersity Δ_{z^H} in z_H is included in the model.

The Caillé structure factor for lamellar systems depends on the total number of layers N, the layer spacing d and the Caillé parameter η, which is a measure for the bilayer fluctuations. The fitting parameters of the model are the total bilayer thickness $l_T = 2(\sigma_H + z_H) \pm \Delta_{z^H}$, ρ_H, ρ_C, σ_C, ρ_{cyl}, N, d and η.

The SAXS data for the elastase was modelled using the software Crysol (Version 2.8 © ATSAS team 1995–2011).[18] Crysol evaluates the solution scattering from macromolecules with known atomic structure. In this work, we used the atomic coordinates for the structure of porcine pancreatic elastase listed in the Protein Databank File pdb file 2V0B.[19]

The form factor for the KA_6E/elastase mixture was modelled using the form factor for generalized flexible Gaussian coils.[20] The parameters of the model are the coil radius of gyration, R_G, the excluded volume parameter from the Flory mean field theory, ν, and a forward scattering at $q = 0$, I_o.

The background for all the SAXS data was fitted according to the modified Porod law $C_1 + \frac{C_2}{q^{C_3}}$, where C_1, C_2 and C_3 are constants.

Fluorescence spectroscopy

Fluorescence spectra were recorded with a Varian Cary Eclipse Fluorescence Spectrometer with samples in 4 mm inner width Quartz cuvettes. Fluorescamine is used as a reagent for the detection of amines because it reacts with primary amines to form highly fluorescent products. The fluorescamine fluorescence assay was performed using (9×10^{-3}–5.6×10^{-2}) wt% KA_6E solutions free of elastase, or containing elastase at a ratio [KA_6E]/[elastase] ~ 300–2000. All the samples contained 0.45 μM fluorescamine. The samples were excited at λ_{ex} = 380 nm, and the fluorescence emission was measured for λ = 410–600 nm.

SDS-PAGE assay

The experiments were performed with >15% polyacrylamide gels. Binary KA_6E/elastase or pure elastase solutions (10 μl) were diluted 1 : 1 in 2 × cc loading buffer containing bromophenol blue, and run on a 15% SDS-PAGE gel. After the run, the gel was stained with Coomassie R overnight, and destained for a day in destaining solution. After imaging, the gel was re-stained using Coomassie G250 (more sensitive staining) overnight, and destained in water for a day before imaging.

Cryo-transmission electron microscopy (cryo-TEM)

Experiments were carried out using a field emission cryo-electron microscope (JEOL JEM-3200FSC) operating at 200 kV. Images were taken using bright-field mode and zero loss energy filtering (omega type) with a slit with 20 eV. Micrographs were recorded using a Gatan Ultrascan 4000 CCD camera. The specimen temperature was maintained at −187 °C during the imaging. Vitrified specimens were prepared using an automated FEI Vitrobot device using Quantifoil 3.5/1 holey carbon copper grids with 3.5 μm hole sizes. Grids were cleaned using a Gatan Solarus 9500 plasma cleaner just prior to use and then transferred into an environmental chamber of FEI Vitrobot at room temperature and 100% humidity. Thereafter, 3 μl of sample solution at 2 wt% concentration was applied on the grid, blotted once for 1 second and then vitrified in a 1/1 mixture of liquid ethane and propane at −180 °C. Grids with vitrified sample solutions were maintained in a liquid nitrogen atmosphere and then cryo-transferred into the microscope.

Transmission electron microscopy (TEM)

TEM imaging was performed using a Philips CM20 TEM microscope operated at 200 kV. Droplets of solutions were placed on Cu grids coated with a carbon film (Agar Scientific, UK), stained with 1 wt% uranyl acetate, and air-dried.

X-ray diffraction (XRD)

X-ray diffraction was performed on a stalk prepared by drying a 43 mM KA_6E gel in Trizma buffer. A solution was suspended between the ends of wax-coated capillaries and dried. The sample-to-detector distance was 50 mm. The stalk was mounted vertically onto the four axis goniometer of a RAXIS IV++ X-ray diffractometer (Rigaku) equipped with a rotating anode generator. The XRD data was collected using a Saturn 992 CCD camera.

Results and discussion

We first examined the self-assembly of KA_6E in comparison to KA_6K in water. FTIR and circular dichroism (CD) spectra, along with TEM images are shown in Fig. 1. The FTIR spectrum for 7 mM KA_6E shows features associated with β-sheet conformation, specifically peaks at 1618 cm^{-1} and 1689 cm^{-1}. The latter is often associated with antiparallel β-sheets. In contrast, even at much higher concentration (300 mM), no ordered conformation was discernible for KA_6K which shows a peaks at 1648 cm^{-1} due to disordered conformation. There is also a peak at 1673 cm^{-1}, which is due to TFA counterions bound to the lysine residues[21] (that this is absent for KA_6E points to the formation of salt bridges between K and E residues on neighbouring peptide molecules). These conclusions are supported by CD spectroscopy since KA_6E shows features associated with β-sheet structures (maximum at 195 nm and minimum at 215 nm) whereas KA_6K shows only a weak maximum near 216 nm, consistent with an extended left-handed helix of polyproline type II.[22] The TEM image shown in Fig. 1c reveals that KA_6E forms fibrils with a diameter of (35.7 ± 2.6) nm at a concentration of 7 mM, whereas at a much higher concentration 300 mM only needle-like aggregates (32.6 ± 3.4 nm) nm thick were observed for KA_6K. These appear to be disordered aggregates as defined spots were not observed by X-ray diffraction (data not shown).

The isoelectric point of KA_6E and KA_6K were calculated to be 10.6 and 6.94 respectively. The pH values for KA_6E and KA_6K in Fig. 1 were 4 and 1 respectively, with a net charge at pH 7 of 0 (KA_6E) and +2 (KA_6K).[23] The increased electrostatic repulsion between KA_6K molecules does not allow for the peptide to form self-assembled fibrils. We will therefore focus in the remainder of this paper on KA_6E which forms β-sheet based fibrils and which undergoes hydrogels. We were motivated to develop enzyme-responsive hydrogels based on KA_6E. We used elastase as enzyme since the alanine-repeat domain in KA_6E is a substrate for this enzyme. Because the proteolytic activity of elastase has an optimum pH of 8.0–8.5,[24] thus further studies were performed in Trizma buffer at pH 8.

KA_6E in Trizma buffer at pH 8 formed solutions at concentrations lower than 42.8 mM and free-standing gels for higher concentrations. The pH of the samples was around 8 for KA_6E concentrations decreasing from 7 to 85.5 mM.

X-ray diffraction was performed to investigate the secondary structure of KA_6E. Similar profiles were obtained from stalks and gels, a representative intensity profile being shown in Fig. 2. As discussed recently for the related peptides A_6R[25] and $A_{12}R_2$,[26] the observed 5.4 Å peak is assigned to the stacking distance of alanine-rich β-sheets (these can pack with a much

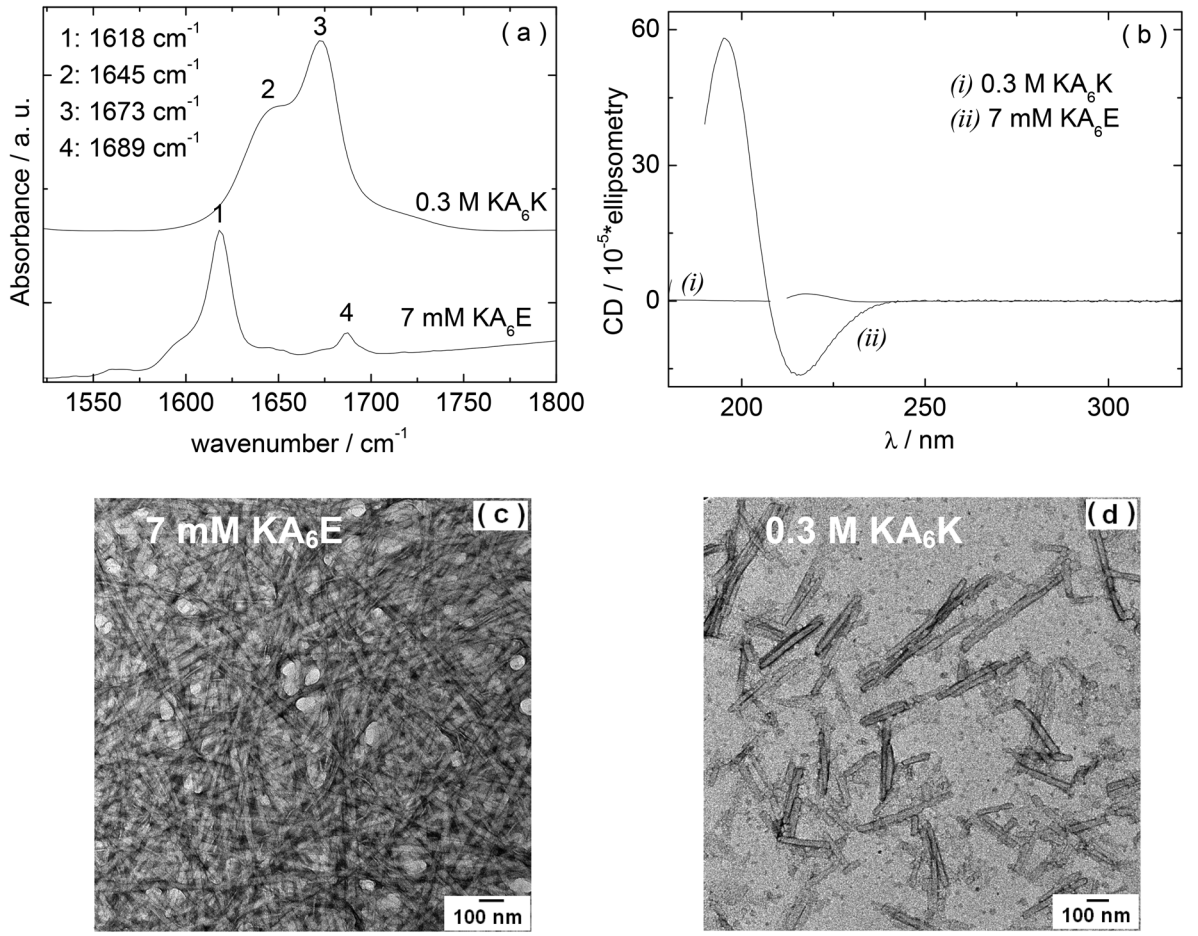

Fig. 1 (a) FTIR spectra, (b) CD spectra (obtained on a Chirascan spectrometer), and (c–d) TEM data obtained for 7 mM KA_6K and 0.3 M KA_6K solutions in water. FTIR data for KA_6K in (a) has been shifted in order to enable the visualization of the data.

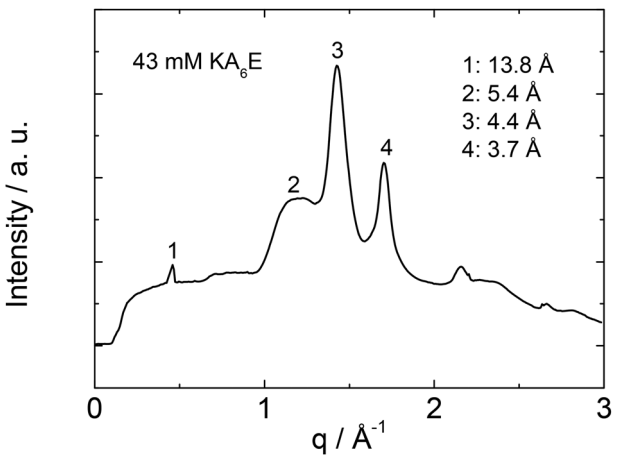

Fig. 2 1D radially averaged profile of the 2D XRD data for a 43 mM KA_6E stalk in Trizma pH 8.

smaller β-sheet spacing than typical for amyloid-forming peptides with other residues in the core β-sheet forming domain[27]). The 4.4 Å peak arises from the peptide strand spacing within the β-sheets[25,26] and the 3.7 Å spacing is associated with diffraction from planes containing the Cα unit.[26] An additional sharp peak is observed with d = 13.8 Å. This is the second order reflection from a layer structure observed by SAXS (*vide infra*). The layer spacing d = 27 Å is consistent with the estimated length of the peptide (8 × 3.4 Å = 27 Å) in an antiparallel β-sheet.[28] This spacing is consistent with an up-down arrangement of the molecules (with no stagger) which is expected to be favoured based on electrostatics (*i.e.* oppositely charged termini are side-by-side).

Fig. 3 shows that KA_6E forms free-standing gels at sufficiently high concentration in Trizma buffer. Upon addition of enzyme at a molar ratio $Mr_E = 2.3 \times 10^3$, de-gelation was observed. $Mr_E = 2.3 \times 10^3$ was selected because under these conditions macroscopic evidence of the gel breakup was observed. This is ascribed to the breakup of the physically entangled fibrillar network, as evidenced shortly through a combination of spectroscopic and microscopic techniques.

CD spectra under similar conditions to those for Fig. 3 are presented in Fig. 4. Similarly to the spectrum in water (Fig. 1), the spectrum for KA_6E in buffer shows β-sheet features, however these are eliminated upon addition of elastase and a spectrum of a disordered peptide conformation is observed. This is consistent with the breakup of the KA_6E fibrils (the CD

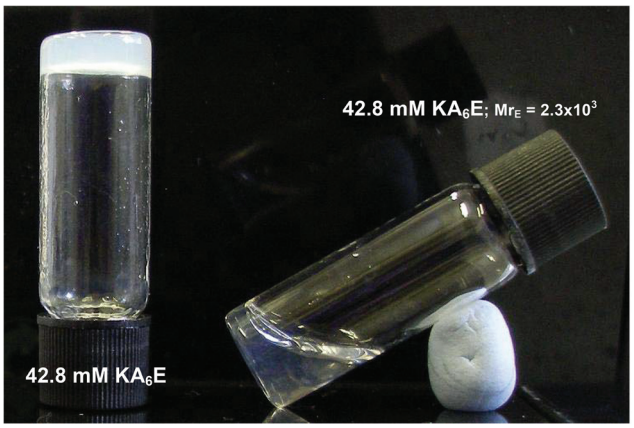

Fig. 3 Free standing gel containing 42.8 mM KA_6E in Trizma pH 8, and solution obtained after adding elastase to a 42.8 mM KA_6E gel at a molar ratio $Mr_E = 2.3 \times 10^3$.

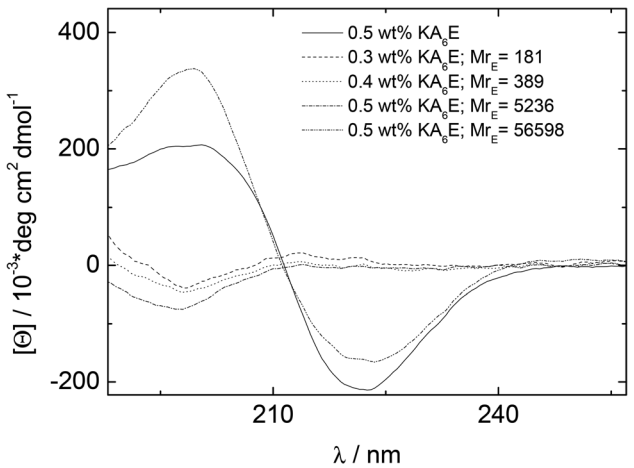

Fig. 4 CD results measured for 0.5 wt% KA_6E Trizma pH 8, and samples containing (0.30–0.5) wt% KA_6E with $Mr_E \sim (180–57000)$.

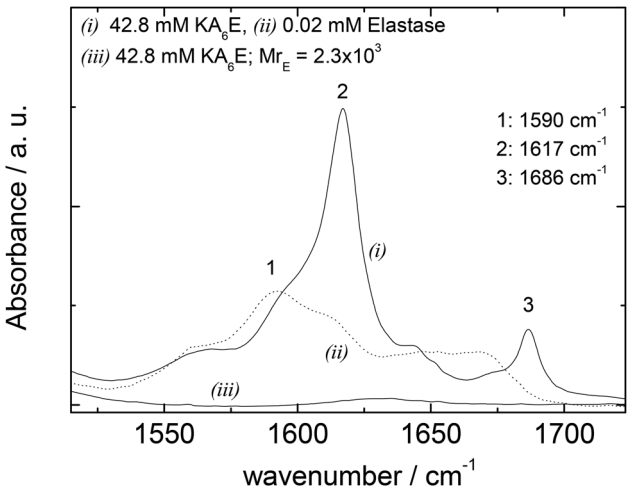

Fig. 5 FTIR data for 42.8 mM KA_6E, 0.02 mM elastase and a mixture (42.8 mM KA_6E; $Mr_E = 2.3 \times 10^3$), in Trizma pH 8.

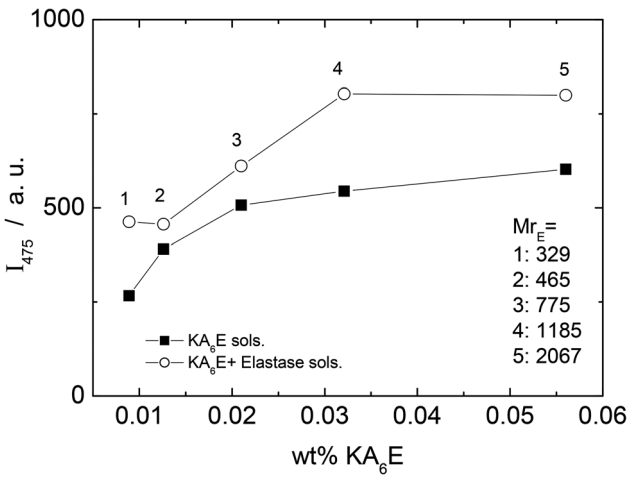

Fig. 6 Fluorescamine assay. Plot of fluorescence emission of fluorescamine at 475 nm *versus* KA_6K concentration with (circle) and without (square) elastase.

spectrum of elastase in water itself does not show strong secondary structure characteristics,[29] and we found the same for elastase in Trizma buffer, data not shown).

FTIR spectra in the amide I′ region shown in Fig. 5 support these conclusions, since the 1617/1686 cm^{-1} β-sheet features disappear on addition of elastase. Elastase itself has predominantly β-sheet structure (*e.g.* PDB file: 3EST),[30] although the FTIR spectrum at 0.02 mM is very weak (Fig. 5).

A fluorescamine fluorescence assay was performed to confirm the existence of free amide groups in the solution. The emission fluorescence spectrum of the fluorescamine was characterised by a broad maxima centred at 475 nm (results not shown). Fig. 6 shows the emission intensity at 475 nm measured for samples containing only KA_6E with 0.45 μM fluorescamine. The results show the existence of free amine groups in the solution, probably because the fluorescamine interacts with the peptide terminus. Fig. 6 also shows the fluorescence for the same KA_6E with 0.45 μM fluorescamine samples, ~30 minutes after adding 1×10^{-3} wt% elastase to them (KA_6E + Elastase, circles). The presence of elastase in solution increases the fluorescence emission at 475 nm, denoting the cleavage of the peptide by the enzyme.[31] The fluorescence measured for control solutions containing 0.45 μM fluorescamine or 1×10^{-3} wt% elastase + 0.45 μM fluorescamine is very weak, and therefore has been omitted in Fig. 6.

Electron microscopy was used to image nanostructures, and the influence of elastase. Fig. 7 shows TEM and separate cryo-TEM images. TEM image in Fig. 7a and b shows that (32.1 ± 8.2) nm thick tapes formed for 7 mM KA_6E (Fig. 7a), are destroyed for 7 mM KA_6E, $Mr_E = 2.3 \times 10^3$ solutions in Trizma pH 8 (Fig. 7b). Similarly, while cryo-TEM images for 14 mM KA_6E show (25 ± 5) nm thick tapes (Fig. 7c), cryo-TEM grids for 14 mM KA_6E, $Mr_E = 2.3 \times 10^3$ solutions were mostly empty (Fig. 7d).

Small-angle X-ray scattering (SAXS) is a powerful *in situ* method to probe self-assembled nanostructures. Synchrotron

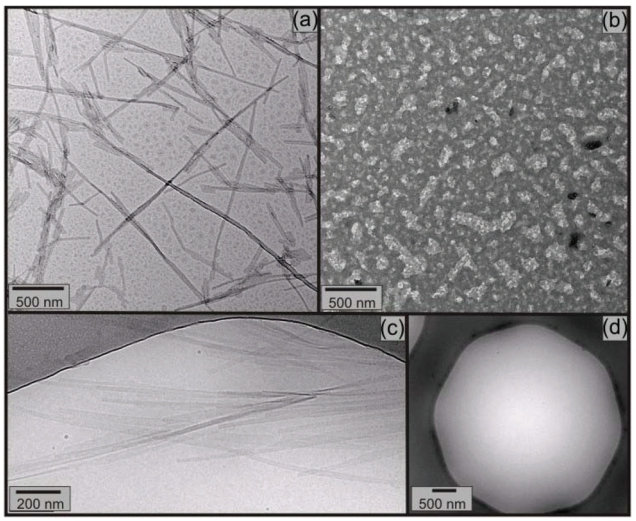

Fig. 7 TEM images obtained for samples dried from (a) 7 mM KA_6E and (b) 7 mM KA_6E; $Mr_E = 2.3 \times 10^3$ solutions in Trizma pH 8. Cryo-TEM images measured for (c) 14 mM KA_6E and (d) 14 mM KA_6E; $Mr_E = 2.3 \times 10^3$ solutions in Trizma pH 8.

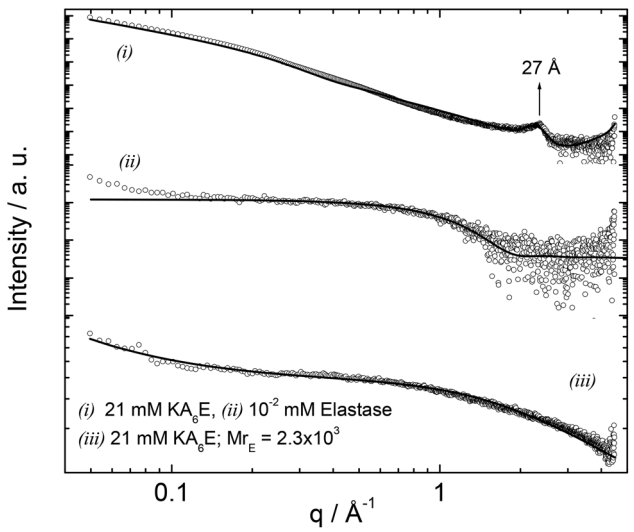

Fig. 8 SAXS curves measured for 21 mM KA_6E, $Mr_E = 2.3 \times 10^3$, in Trizma pH 8 and the corresponding controls. The full lines represent the fitting to the data as described in the text.

SAXS was used to investigate the structure of KA_6E in buffer with and without elastase. Fig. 8 shows the data along with model fits to the form factor intensity profiles. For KA_6E, which forms β-sheets stacking into tape-like fibrils, we used a model of a Gaussian bilayer with a structure factor corresponding to the Caillé model of multi-layer systems. We have recently used this model to describe the SAXS profile from several peptide amphiphiles, and further details of the model can be found in these papers.[32] The peak at $q = 0.23^{-1}$ corresponds to a spacing $d = 27$ Å, as mentioned above a second order reflection associated with this spacing is identified by XRD. This periodicity is equal to the estimated length of the KA_6E molecule and from this we infer up-down side-side stacking of the molecules within a layered structure. The parameters obtained from the fit of the SAXS data are listed in Table 1.

The form factor of elastase was computed from the published crystal structure (as described in the SAXS Theory section). It agrees very well with the data. Upon addition of elastase, the fibrils break up (as confirmed by TEM and spectroscopic techniques discussed above), therefore the form factor was fitted using a Gaussian coil model already described in the Experimental section. The parameters obtained from the SAXS fit are listed in Table 1.

The products of KA_6E cleavage by elastase were analyzed using SDS-PAGE, a technique that separates molecules (peptides) according to their mass. Due to the fact that KA_6E has a mass lower than 10 kDa, this technique only gives broad information on the mass of the PA and its cleaved fragments. In addition, gels with a high percentage of polyacrylamide (15%) were used (Fig. 9). The undigested peptide (lane 1) was not observed in the expected region of migration (~1 kDa), probably due to limitations of the technique. In particular, we were not able to run molecular markers with masses comparable to those of the PA, whereas the front of sample migration (*i.e.*, migration of bromophenol blue) is around 5 kDa. Despite this, bands were observed at 60 and 30 kDa (bands a and b) which may be due to peptide aggregates. These bands were not present for the peptide/elastase mixture in lane 2, but were detected in lane 3 (peptide/elastase with lower concentrations of both KA_6E and elastase). The elastase enzyme (lane 4) appeared as three separate bands, one at ~25 kDa (c) and what were probably autocleavage products of ~15 + 8 + 5 kDa (d + e + f, respectively). The same pattern is also evident in lane 2, where a greater amount of elastase was added to the peptide. In summary, SDS-PAGE suggests that peptide aggregates seem to disappear after incubation with higher elastase concentrations, which provides indirect evidence of KA_6E cleavage. Electrospray mass spectrometry data (not shown) also confirmed cleavage of the peptide, with a strong peak at $m/z = 431$ which is assigned to a fragment KA_4 or A_4E.

Table 1 SAXS parameters extracted from the fittings of the experimental data shown in Fig. 8

Sample	l_T [Å]	ρ_H [rel. units]	ρ_C [rel. units]	σ_C [Å]	N	d [Å]	η	R_G [Å]	ν_1	I_o [rel. units]	C_2 [rel. units]	C_3
21 mM KA_6E	30.6 ± 4.58	2×10^{-4}	3.5×10^{-4}	5.3	4	27	0.1	—	—	—	8	2
21 mM KA_6E; $Mr_E = 2.3 \times 10^3$	—	—	—	—	—	—	—	7	1	38.8	0.7	1.2

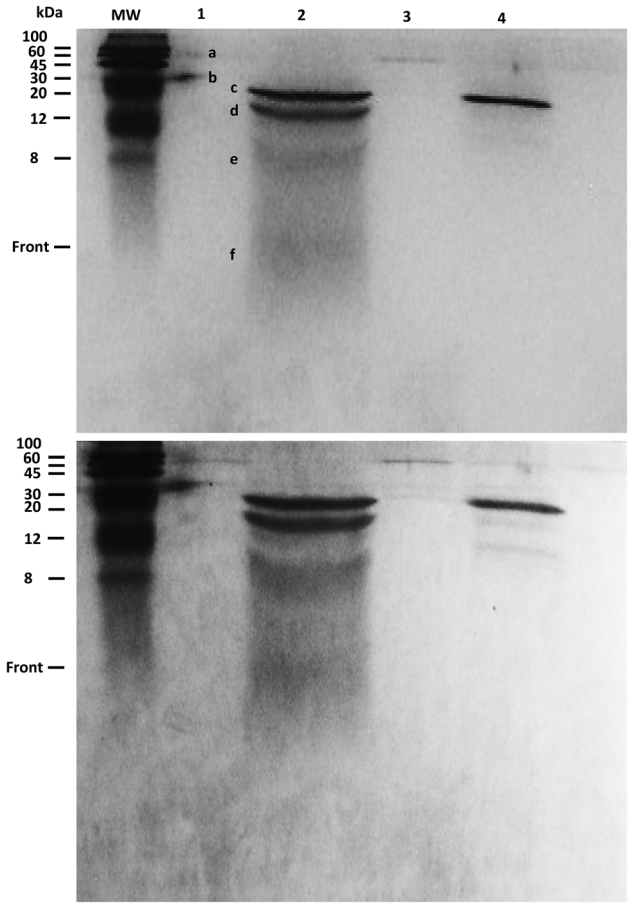

Fig. 9 SDS-PAGE assay run for 15% polyacrylamide gel stained with Coomassie R (upper) or G250 (lower panel). Bands were detected on lane 1(a–b), 2(c–d and f), 3(a–c) and 4 (a–e). Lane 1: 1.5 wt% KA_6E, Lane 2: 1.5 wt% KA_6E + 0.026 wt% elastase (Mr_E = 2129), Lane 3: 0.0062 wt% KA_6E + 0.00011 wt% elastase (Mr_E = 2080), Lane 4: 0.13 wt% elastase.

Conclusions

The self-assembly of two telechelic amphiphilic peptides has been studied in aqueous solution. The di-cationic peptide KA_6K does not self-assemble in aqueous solution over the extensive range of concentrations examined, instead the formation of crystals is observed at higher concentration. The inability of KA_6K to form self-assembled structures such as β-sheet fibrils is ascribed to unfavourable repulsion between the terminal lysine residues.

In complete contrast, favorable interactions between the termini in the catanionic peptide KA_6E enable self-assembly into tape-like fibrils at low concentration. The fibrils comprise layers a single molecule thick of KA_6E molecules, presumably arranged in an up-down side-to-side arrangement due to favorable electrostatic interactions between the oppositely charged termini as suggested by XRD data.

At a sufficiently high concentration, hydrogelation is observed for KA_6E, which is driven by the formation of a fibrillar network structure. The enzymatic degradation of the hydrogel by elastase, for which alanine repeat sequences are substrates, was observed. SDS-PAGE and TEM indicate that peptide aggregates are disrupted in the presence of the enzyme whilst at a molecular level FTIR, CD and SAXS show the breakup of the self-assembled β-sheet fibrillar nanostructure.

Given its remarkably simple design and short peptide sequence, KA_6E may serve as a useful model system for further studies of elastase degradation. In further work, we also plan to investigate the biocompatibility of the hydrogels and their use in topical applications. Potential applications in regenerative medicine, associated with the selective uptake of elastase (which disrupts collagen leading to tissue degeneration), will also be explored.

Acknowledgements

This work was supported by BBSRC grant BB/I008187/1. We acknowledge access to the Chemical Analysis Facility at the University of Reading. We are grateful to the ESRF for the award of beamtime on BM29 (ref. MX-1511) and to Adam Round for assistance with the SAXS experiments.

References

1 (*a*) B. K. Mann, A. S. Gobin, A. T. Tsai, R. H. Schmedlen and J. L. West, *Biomaterials*, 2001, **22**, 3045–3051; (*b*) J. J. Rice, M. M. Martino, L. De Laporte, F. Tortelli, P. S. Briquez and J. A. Hubbell, *Adv. Healthcare Mater.*, 2013, **2**, 57–71.
2 A. Janoff, *Annu. Rev. Mater. Res.*, 1985, **36**, 207–216.
3 N. J. Trengove, M. C. Stacey, S. Macauley, N. Bennett, J. Gibson, F. Burslem, G. Murphy and G. Schultz, *Wound Repair Regen.*, 1999, **7**, 442–452.
4 C. M. Bellingham, M. A. Lillie, J. M. Gosline, G. M. Wright, B. C. Starcher, A. J. Bailey, K. A. Woodhouse and F. W. Keeley, *Biopolymers*, 2003, **70**, 445–445.
5 S. Marqusee, V. H. Robbins and R. L. Baldwin, *Proc. Natl. Acad. Sci. U. S. A.*, 1989, **86**, 5286–5290.
6 J. Makowska, S. Rodziewicz-Motowidlo, K. Baginska, J. A. Vila, A. Liwo, L. Chmurzynski and H. A. Scheraga, *Proc. Natl. Acad. Sci. U. S. A.*, 2006, **103**, 1744–1749.
7 A. S. Gobin and J. L. West, *FASEB J.*, 2002, **16**, 751.
8 (*a*) B. L. Thiel, K. B. Guess and C. Viney, *Biopolymers*, 1997, **41**, 703–719; (*b*) B. An, J. E. Jenkins, S. Sampath, G. P. Holland, M. Hinman, J. L. Yarger and R. Lewis, *Biomacromolecules*, 2013, **13**, 3938–3948.
9 (*a*) S. Vauthey, S. Santoso, H. Gong, N. Watson and S. Zhang, *Proc. Natl. Acad. Sci. U. S. A.*, 2002, **99**, 5355–5360; (*b*) X. B. Zhao, F. Pan, H. Xu, M. Yaseen, H. H. Shan, C. A. E. Hauser, S. G. Zhang and J. R. Lu, *Chem. Soc. Rev.*, 2010, **39**, 3480–3498.
10 H. G. Cui, E. T. Pashuck, Y. S. Velichko, S. J. Weigand, A. G. Cheetham, C. J. Newcomb and S. I. Stupp, *Science*, 2010, **327**, 555–559.

11 V. Castelletto, D. Nutt, I. W. Hamley, S. Bucak, C. Cenker and U. Olsson, *Chem. Commun.*, 2010, **46**, 6270–6272.
12 S. Bucak, C. Cenker, I. Nasir, U. Olsson and M. Zackrisson, *Langmuir*, 2009, **25**, 4262–4265.
13 J. Madine, V. Castelletto, I. W. Hamley and D. A. Middleton, *Angew. Chem.*, 2013, **52**, 10537–10540.
14 A. Fujie, T. Komoto, M. Oya and T. Kawai, *Makromol. Chem.-Macromol. Chem. Phys.*, 1973, **169**, 301–321.
15 (*a*) J. Makowska, K. Baginska, A. Skwierawska, A. Liwo, L. Chmurzynski and H. A. Scheraga, *Biopolymers*, 2008, **90**, 772–782; (*b*) Z. S. Shi, C. A. Olson, G. D. Rose, R. L. Baldwin and N. R. Kallenbach, *Proc. Natl. Acad. Sci. U. S. A.*, 2002, **99**, 9190–9195; (*c*) K. Chen, Z. G. Liu and N. R. Kallenbach, *Proc. Natl. Acad. Sci. U. S. A.*, 2004, **101**, 15352–15357.
16 R. Hussain, T. S. Javorfi and G. Siligardi, *J. Synchrotron Radiat.*, 2012, **19**, 132–135.
17 (*a*) G. Pabst, M. Rappolt, H. Amenitsch and P. Laggner, *Phys. Rev. E: Stat. Phys., Plasmas, Fluids, Relat. Interdiscip. Top.*, 2000, **62**, 4000–4008; (*b*) A. Caille, *C. R. Seances Acad. Sci., Ser. B*, 1972, **274**, 891–893; (*c*) R. Zhang, R. M. Suter and J. F. Nagle, *Phys. Rev. E: Stat. Phys., Plasmas, Fluids, Relat. Interdiscip. Top.*, 1994, **50**, 5047–5060.
18 (*a*) M. V. Petoukhov, D. Franke, A. V. Shkumatov, G. Tria, A. G. Kikhney, M. Gajda, C. Gorba, H. D. T. Mertens, P. V. Konarev and D. I. Svergun, *J. Appl. Crystallogr.*, 2012, **45**, 342–350; (*b*) D. Svergun, C. Barberato and M. H. J. Koch, *J. Appl. Crystallogr.*, 1995, **28**, 768–773.
19 J. Jakoncic, db file 2V0B. DOI: 10.2210/pdb2v0b/pdb.
20 M. Born and H. S. Green, *Proc. R. Soc.*, 1946, **A188**, 10–18.
21 (*a*) H. Gaussier, H. Morency, M. C. Lavoie and M. Subirade, *Appl. Environ. Microbiol.*, 2002, **68**, 4803–4808; (*b*) J. T. Pelton and K. R. McLean, *Anal. Biochem.*, 2000, **277**, 167–176.
22 (*a*) A. F. Drake, G. Siligardi and W. A. Gibbons, *Biophys. Chem.*, 1988, **31**, 143–146; (*b*) G. Siligardi and A. F. Drake, *Biopolymers*, 1995, **37**, 281–292.
23 http://www.innovagen.se, in 2013.
24 (*a*) J. Bieth, B. Spiess and C. G. Wermuth, *Biochem. Med.*, 1974, **11**, 350–357; (*b*) J. Bieth, in *Elastases: Structure, Function and Pathological Role*, ed. J. Bieth, G. Collin-Lapinet and L. Robert, Basel, 1978.
25 I. W. Hamley, A. Dehsorkhi and V. Castelletto, *Chem. Commun.*, 2013, **49**, 1850–1852.
26 I. W. Hamley, A. Dehsorkhi, V. Castelletto, J. Seitsonen, J. Ruokolainen and H. Iatrou, *Soft Matter*, 2013, **9**, 4794–4801.
27 L. C. Serpell, *Biochim. Biophys. Acta, Bioenerget.*, 2000, **1502**, 16–30.
28 T. E. Creighton, *Proteins. Structures and Molecular Properties*, W.H. Freeman, 1993.
29 L. Visser and E. R. Blout, *Biochemistry*, 1971, **10**, 743–752.
30 E. Meyer, G. Cole, R. Radhakrishnan and O. Epp, *Acta Crystallogr., Sect. B: Struct. Sci.*, 1988, **44**, 26–38.
31 A. A. Aimetti, M. W. Tibbitt and K. S. Anseth, *Biomacromolecules*, 2009, **10**, 1484–1489.
32 (*a*) V. Castelletto, G. Cheng, C. Stain, C. J. Connon and I. W. Hamley, *Langmuir*, 2012, **28**, 11599–11608; (*b*) V. Castelletto, R. J. Gouveia, C. J. Connon and I. W. Hamley, *Faraday Discuss.*, 2013, **166**, 381–397.

